Loading Precursors into Self-Assembling Contacts for Improved Performance and Process Control in Evaporated Perovskite Solar Cells

Matthew R. Leyden, Viktor Škorjanc, Aleksandra Miaskiewicz, Stefanie Severin, Suresh Maniyarasu, Thomas Gries, Johannes Beckedahl, Florian Scheler, Maxim Simmonds, Philippe Holzhey, Jona Kurpiers, Lars Korte, Marcel Roß,* and Steve Albrecht**

Organo-lead-halide perovskites are promising materials for solar cell applications with efficiencies now exceeding 26% for single junction, and over 33% for silicon tandem devices. Evaporation has proven viable for industrial scale-up but presents challenges for perovskite materials. Perovskite precursor is introduced into self-assembling MeO-2PACz hole transport layers for application to 4 source perovskite coevaporation. This allows precursors that can be difficult to add via evaporation, like methylammonium chloride. These precursor molecules influence growth during evaporation, film behavior during annealing as measured by photoluminescence, and aid the conversion to perovskite as shown by X-Ray diffraction. Devices have improved power conversion efficiency and stability compared to a control sample within the same evaporation. The best cells reach ≈21% efficiency and comparable performing ≈20% cells maintain their original efficiency after 1000 h of maximum power tracking at 25 °C. This process provides significant process flexibility for perovskite evaporation and requires no additional steps.

1. Introduction

Perovskite materials such as metal-halide perovskites show great potential in optoelectronic applications, most notably as a solar cell absorber material. Their higher absorption coefficient allows thinner absorber layers (<1 μm).[1] The carrier mobility of many perovskites is relatively balanced and good enough to yield fast carrier extraction for thin-film solar cells. These desirable attributes have allowed perovskite materials to demonstrate certified photo conversion efficiencies (PCE) up to ≈26.5%.[2,3] This is comparable to the best single-crystal solar cell (27.3%).[2] Perovskites have the highest efficiency among thin film solar cells, exceeding copper indium gallium selenide (CIGS—23.6%) and cadmium telluride (CdTe—22.6%).[2] Perovskites are characterized by an octahedral crystal structure and ABX_3 stoichiometry, where A is a cation, B is often a metal, and X is an anion. Most recent attention has been on lead- or tin-based perovskites, where the anion is iodide, bromide, or chloride. The highest-performing perovskite solar cells typically use an organic cation like formamidinium (FA) or methylammonium (MA), but the inorganic material cesium is also often used. In addition, mixtures of the different A, B, or X-sites allow fine-tuning of the bandgap.[4]

There are several ways to fabricate perovskite solar cells, common methods include solution processing and coevaporation. Evaporation has a few advantages compared to solution processing, especially in application of perovskites to tandem solar cells, where perovskites can complement an established technology. Perovskites have a tunable bandgap and can be optimized to be compatible with the corresponding bottom cell, and silicon tandems have demonstrated efficiencies of 33.9%.[2] Silicon solar cells are often textured with pyramids that better help capture light. However, if pyramids are too large (greater than 1 μm), it can be challenging for solution deposition to achieve a pinhole-free film. This limitation can be alleviated by using smaller random pyramids.[5] Evaporated perovskites are highly conformal and can be deposited on high aspect ratio surfaces like random pyramids.[6] Furthermore, evaporated perovskites do not use toxic solvents like dimethylformamide (DMF) for precursors, or antisolvents like chlorobenzene.[7,8] Additionally, the commonly used solvent dimethyl sulfoxide (DMSO) has been linked to the rapid degradation of perovskite solar cells.[9] Evaporated perovskites can be patterned by shadow masking, which potentially skips post-patterning steps such as laser ablation. Evaporation is a proven technology for many industrial applications. Evaporated films do not experience the severe edge

M. R. Leyden, V. Škorjanc, A. Miaskiewicz, S. Severin, S. Maniyarasu, T. Gries, J. Beckedahl, F. Scheler, M. Simmonds, P. Holzhey, J. Kurpiers, L. Korte, M. Roß, S. Albrecht
Perovskite Tandem Solar Cell Group
Helmholtz-Zentrum Berlin
Kekuléstraße 5, 12489 Berlin, Germany
E-mail: matthew.leyden@helmholtz-berlin.de; marcel.ross@helmholtz-berlin.de; steve.albrecht@helmholtz-berlin.de

The ORCID identification number(s) for the author(s) of this article can be found under https://doi.org/10.1002/solr.202400575.

DOI: 10.1002/solr.202400575

effects seen in solution processing, and can transition to larger area substrates without significantly changing process conditions.[10] Evaporated CdTe solar cells are the dominant thin film solar technology, and in part, have been successful because of high deposition rates ≈10 μm min^{-1}.[11] Recently efficiencies from evaporated processes have become competitive, where sequential evaporation techniques are now on par with the best solution-processed cells (PCE of 26.1%).[12] This demonstration of high efficiency and its intrinsic advantages show promise for the evaporation of perovskite solar cells.

For all its advantages, perovskite evaporation is not without its challenges. Perovskite evaporation can be two orders of magnitude slower than spin coating in terms of fabrication time due to limited evaporation rates. Second, evaporation is less commonly used due to higher capital equipment costs. Industrially relevant evaporation equipment can cost millions of dollars.[11] Third, it can be challenging to incorporate new materials into an evaporation process. A new material typically requires a new evaporation source, adding complexity. Furthermore, many desirable materials may not evaporate easily (e.g., because they are too volatile), making a process difficult to control.[13,14] Molecules used in low-dimensional perovskites (Dion–Jacobson, or Ruddlesden-Popper perovskite) may stabilize and passivate perovskite films.[15] These passivating cations are frequently used at concentrations much lower than other cations, which can be challenging to deposit correctly by codeposition due to rate sensor error and cross talk. These challenges facing evaporated perovskites are not insignificant, however, we will show in this paper that loading transport layers with perovskite precursor can improve performance and provide new possibilities in evaporated perovskite processes.

Molecules like (2-(3,6-Dimethoxy-9H-carbazol-9-yl)ethyl) phosphonic acid (MeO-2PACz) can form self-assembled monolayers (SAMs) or self-assembling contacts. The phosphonic acid tail binds to hydroxyl groups on the surface of the transparent conducting oxide (e.g., indium tin oxide—ITO) used for solar cells. Carbazole-based SAM molecules have gained popularity as robust hole transport layers (HTLs) for perovskite solar cells.[16] As shown in **Figure 1**, as-spun films of SAM are often not a literal monolayer. A monolayer is only formed if the solution concentration is low, or the subsequent film is rinsed. Solution-based perovskite deposition techniques effectively wash off SAM molecules that have not formed strong bonds to the substrate. In evaporated processes, these loosely bound SAM molecules can affect how perovskite films are formed.[6] However, this influence of the SAM on the perovskite growth is not the only factor determining film quality. Our baseline process using SAM-based HTLs is sensitive to small variations in evaporation conditions, which can significantly impact solar cell performance. A robust process with a wide process window is important for industrialization. Therefore, a substrate that better defines film growth is advantageous to reproducibility.

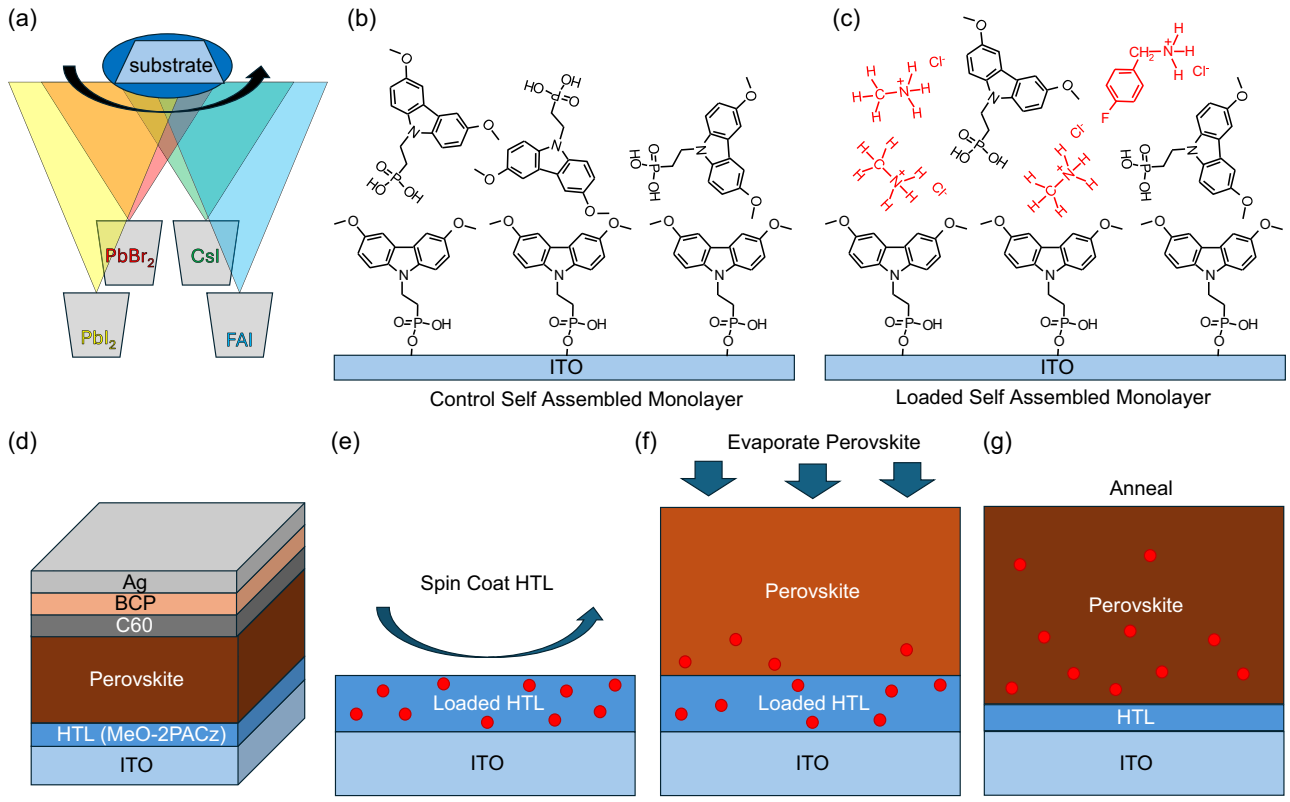

Figure 1. L-HTLs incorporate perovskite precursors into evaporated perovskite films to improve performance. a) Diagram of a 4-source perovskite codeposition. b) Sketch of an as-spun MeO-2PACz HTL. c) Sketch of a loaded transport layer containing perovskite precursor molecules (here: MACl, FBACl). d) Structure of our perovskite solar cell. e) Sketch of the deposition process using a loaded transport layer, with perovskite precursor represented as red dots, f) with a subsequently evaporated perovskite film, and g) an annealed film, which has incorporated precursors into the perovskite film.

A recent publication used a method of pre-embedding a tin oxide electron transport layer with formamidinium iodide (FAI) and CsBr for sequentially spin-coated perovskite solar cells.[17] This method improved the efficiency of solar cells, reduced the concentration of lead iodide at their buried interface, and reduced the strain of the subsequent perovskite films. We independently developed an analogous approach of loading perovskite precursor molecules into self-assembling contacts to provide flexibility for perovskite evaporation. We will refer to this film as a loaded hole transport layer (L-HTL).

2. Results and Discussion

To create a L-HTL, perovskite precursor material is added to the solution of the HTL. The as-spun film contains MeO-2PACz and perovskite precursor but still functions as a hole-transporting layer. The precursor material from the HTL can diffuse into a subsequently evaporated perovskite film. Anything that is cosoluble with the SAM molecules can potentially be used. This requires no additional processing step, or additional sources in the evaporator, and can include materials that are otherwise undesirable to deposit via evaporation. Below, we demonstrated the precursor methylammonium chloride (MACl) in L-HTLs, which is comparatively more volatile than other perovskite organic cations. Additionally, we included a small portion of 4-fluoro-benzylammonium chloride (FBACl), which can be difficult to deposit by coevaporation. Larger cations like FBACl are widely reported to increase photoluminescent yield and improve the stability of solar cells.[15] L-HTLs allow the perovskite evaporation community to apply materials that previously may have only been used by solution processing. The process of pre-embedding is comparable to our use of an L-HTL, however, the motivations to pursue a loaded transport layer differs here in application to evaporated perovskites.

We used 4-source coevaporation to deposit perovskite films, which included lead iodide, lead bromide, cesium iodide, and formamidinium iodide. Using this set of materials, we can potentially tune the perovskite bandgap, ranging from a low bandgap of $FAPbI_3$ (≈1.5 eV) to $CsPbIBr_2$ (≈2 eV). Our baseline coevaporation process is described in the Supporting Information. Based on rates and tooling factors, we estimate our composition to be $FA_{0.8}Cs_{0.2}PbI_{2.7}Br_{0.3}$, or ≈11% bromide, and a final thickness of ≈700 nm. We measured perovskite films using X-Ray photoelectron spectroscopy to measure the relative chemical composition (XPS, Table S1, Supporting Information). The ratios measured by XPS approximately agree with the ratios estimated from our tooling factors. However, the XPS measurement showed concentrations of FA and iodide at the surface were lower than what we would expect from tooling factors.

The amount of lead iodide formed in a coevaporated film can depend on the concentration of MeO-2PACz solutions.[6] Thinner films of MeO-2PACz resulted in perovskite films with more lead iodide, suggesting a deficiency in FAI during evaporation. Another report claimed that the phosphonic acid groups on MeO-2PACz aided the capture of FAI for coevaporated perovskites. A monolayer SAM (no loosely bound MeO-2PACz) required coevaporating ≈30% more FAI than films using a thick MeO-2PACz HTL.[18] This strong dependence on the substrate surface suggests perovskite formation happens at the surface, rather than as a pure vapor-based reaction. MeO-2PACz may template a perovskite structure that facilitates continued capture of FAI. Alternatively, the MeO-2PACz might stay at the top surface of the growing film, continuing to facilitate FAI capture during deposition. We have found that only using thicker films of MeO-2PACz is not always sufficient to capture enough FAI for proper and consistent growth. Also, simply increasing the deposition rate of FAI is not an effective strategy as solar cell performance is negatively impacted by FAI excess. A robust process that is tolerant to variations in FAI ambient pressure and deposition rates, would lead to more consistent solar cell production. Therefore, we developed the strategy of loaded HTLs.

For initial trials, we loaded HTLs with MACl at concentrations of 4 and 16 mM, with a concentration of MeO-2PACz of 4 mM. The precursor MACl is commonly used for high-performance solution-processed solar cells.[5] Initially, it was unclear if the SAM would properly function as a minority solute (i.e., more MACl than MeO-2PACz), and if loading the solution would interfere with SAM film formation. We measured the thickness of the spun film with and without loading via ellipsometry. We found the thickness of the film remained approximately unchanged at ≈5 nm, even for the higher concentration of 16 mM of MACl (Supporting Information Methods). This was surprising but may be reasonable considering that MACl is a smaller molecule than MeO-2PACz. We can place an upper bound on the inclusion of MACl if we assume that the entire HTL film (≈5 nm) is only made of MACl. The reports on the density of MACl vary, here we use $0.49\ g\ cm^{-3}$.[19] Assuming FAI is added until perovskite forms a stoichiometrically balanced film, this 5 nm of MACl would make up a ≈1% molar fraction of the cation in the resultant perovskite film. This is only an estimate but provides an order of magnitude to base expectations. As will be shown, a small fractional change in cation concentration can offer a significant improvement in perovskite film performance.

We can gain insight into the growth process by measuring the in situ photoluminescence (PL) during evaporation. The PL emitted from the perovskite layer from the first 5 min of growth is shown in **Figure 2**. Once the shutter is open the perovskite nucleates on the substrate emitting at a high bandgap of ≈1.8 eV. The bandgap then rapidly decreases in the first few minutes of deposition. As the deposition progresses, typically this shift will slow down. A bandgap of 1.8 eV is higher than expected from the nominal stoichiometry. This initial high bandgap may be from weak quantum confinement effects as the film is thin (≈3–10 nm), and likely forming islands. The bandgap and size (thickness) range are comparable to iodide-based low-D perovskite single crystals (e.g., $n = 4$, 1.87 eV, ≈6 nm).[20] Once the film gets thicker the bandgap stabilizes, likely resembling bulk behavior. Alternatively, there could be some initial preferential nucleation of high bromide perovskite, which will be the subject of further investigation.

We compare the control film to one using a loaded transport layer, where we see similar behavior, except the PL relaxes to a lower bandgap value (Figure 2b). Films loaded with MACl often result in lower bandgap perovskite. This may partially be due to the change in the nucleation behavior during the first few minutes of deposition shown in Figure 2b. Figure S1a, Supporting Information, additionally shows the in situ PL from

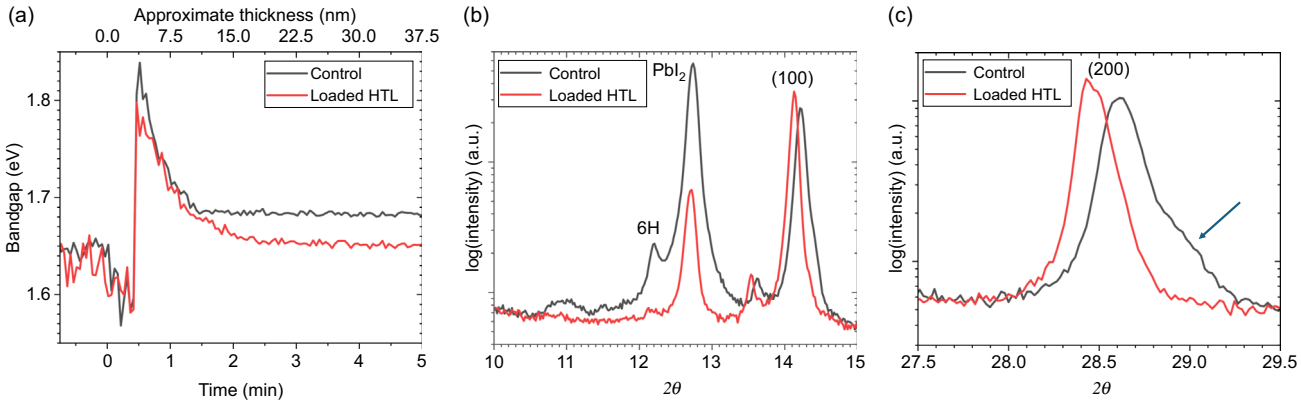

Figure 2. Films using loaded transport layers form a lower bandgap perovskite more quickly and yield a more phase pure perovskite. a) In situ PL from a 4-source evaporation on a control MeO-2PACz substrate, and one loaded with 4 mM MACl. Time zero is set when the shutter is opened. The bandgap as measured by peak PL position for the first few minutes. b,c) XRD patterns from annealed films from a control and an L-HTL with MACl and FBACl: (b) X-Ray diffraction patterns show reduced peaks for the undesirable crystal phases of lead iodide and the 6H polytype. (c) The patterns also show a shift in the (200) peak of perovskite using an L-HTL and the absence of the shoulder seen in the control (arrow).

a growth using a washed SAM. The washing should remove most MeO-2PACz not covalently bonded to the ITO. Perovskite grown on this washed film has a PL that shifts to lower bandgaps more slowly, corroborating the idea that excess MeO-2PACz helps with FAI absorption. The PL intensity will often increase with film thickness but appears to saturate when the film is approximately a few hundred nanometers thick and can absorb most of the light. However, sometimes we see an abrupt drop in the PL intensity (Figure S1b, Supporting Information). This drop is possibly from high strain in the perovskite during growth, and a restructuring of the film that results in loss of PL intensity. Alternatively, this drop in PL originates from a change in deposition conditions that leads to higher defect density.

We used X-Ray diffraction (XRD) to measure the composition of the crystalline component within our perovskite thin films. We compared the crystal structure of a perovskite using an L-HTL (6 mM MACl and 0.6 mM FBACl) with a control sample with only MeO-2PACz (Figure 2c,d, and Figure S2, Supporting Information). The largest difference in these patterns is that the control sample had a more pronounced lead iodide peak ($2\theta \approx 12.7°$). This suggests a more significant fraction of lead iodide remained unconverted for the control sample. The film using an L-HTL had a comparatively small lead iodide peak, which is expected from adding A site precursor. In the pattern of the control film, there is a small peak at ≈12.2°, which we associate with a hexagonal phase (6 H) of $(FAPbI_3)_x(MAPbBr_3)_{1-x}$ perovskite.[21] Additionally, the phases of 4 H and 2 H may also be present at 11.6° and 11.8° but are much less pronounced. These hexagonal polytypes are correlated with more rapid degradation of perovskite.[22] These polytypes are largely absent in patterns from the film using an L-HTL, suggesting that it should be less prone to degradation. This improvement in the crystal structure may be from the inclusion of MACl, which is reported to assist in reducing the formation of these polytype phases.[23] The (200) perovskite peak ($2\theta \approx 28.6°$ and ≈28.4° for control and L-HTL) is shifted to a lower value for the L-HTL samples, which suggests a larger lattice parameter and smaller bandgap.[24] Indeed, the bandgap measured by PL for the control was ≈1.65 and ≈1.62 eV for the L-HTL. Additionally, we can see a shoulder on this peak for the control sample, indicating phase heterogeneity, likely from higher bromide content material. This feature was not in the L-HTL sample, indicating homogeneity and improved film quality. The addition of bulky cations like FBACl can lead to the formation of low-dimensional perovskite, even when the average order is relatively high.[25] However, it is used here in low enough concentrations that we see no direct evidence of such a phase from XRD or PL, and the molecule predominantly exists on the surface of bulk perovskite.

XRD diffractograms showed that the L-HTL appears to help complete conversion to perovskite, and is consistent with our scanning electron microscope (SEM) images. We use SEM as a technique to measure surface morphology and identify changes in composition. From previous experience and existing literature,[26] we believe SEM can be used to identify lead iodide at the surface. **Figure 3**a–f shows a perovskite film loaded with 4 mM (MACl) compared to a control film evaporated in the same batch. In the control sample, we observe what appear to be lead iodide crystals on the top surface.[26] These crystals are largely absent in the L-HTL sample, suggesting a more complete conversion to perovskite. Additionally, we measured the thickness of the films shown in the SEM images to be ≈640 nm for the L-HTLs and ≈590 nm for the control. The thickness of the samples as measured by a profilometer was ≈670 nm for the L-HTL and ≈660 nm for the control. The differences in thickness by technique may reflect averaging over a larger area by the profilometer. This increase in thickness when using L-HTLs is also consistent with a volume expansion from lead halide to perovskite. This volume increase is seen in publications using sequential deposition.[27] The thicker perovskite using the L-HTL film is consistent with a more complete conversion to perovskite. Again, control samples typically had some lead iodide as observed by SEM and XRD. There are reports of an improvement in performance with some fraction of lead iodide. For example, increasing the excess of lead iodide leads to increased open circuit voltage in evaporated perovskites.[28] The perovskite evaporation recipe reflects earlier iterations of solar cell performance optimization.

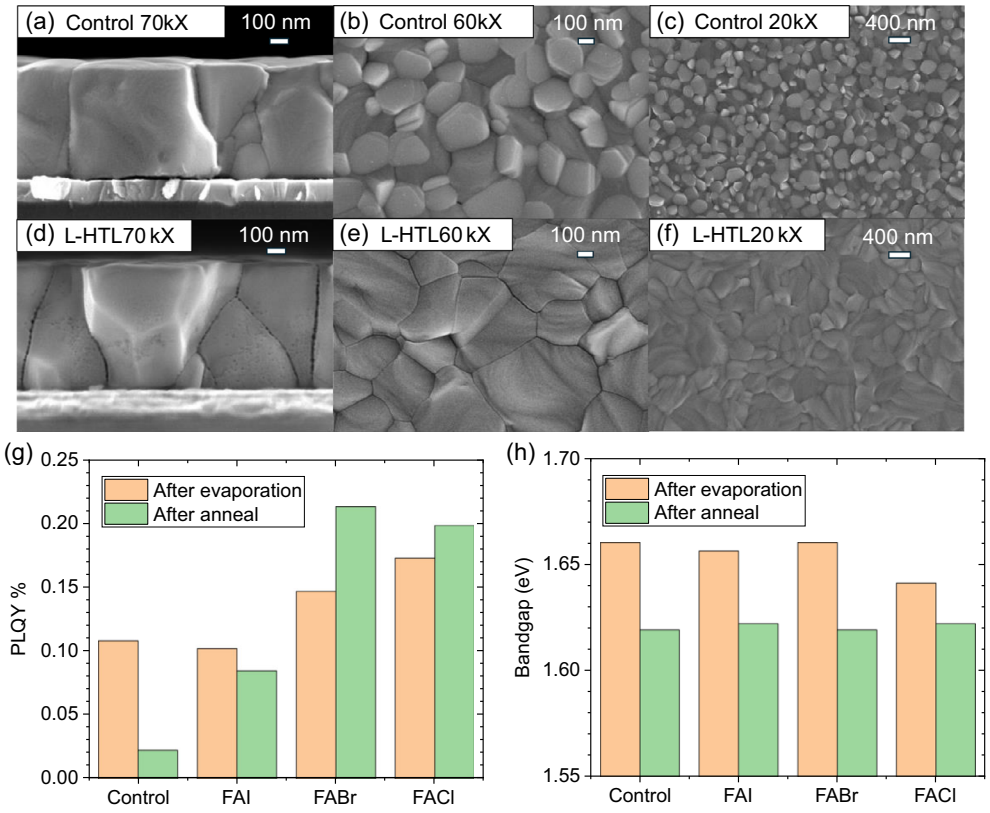

Figure 3. Loaded transport layers provide a more complete conversion of lead halide to perovskite with higher PLQY. a–c) SEM images from the control film, and d–f) images of a film created using an L-HTL with 4 mM MACl, both films were prepared during the same evaporation. The cross sections in (a) and (d) reveal a slightly thicker film for the L-HTL (≈640 nm) compared to the control (≈590 nm). Images (b) and (c) show apparent lead iodide crystals on the control sample that are absent in the L-HTL sample (e) and (f). g) PLQY and h) bandgap as measured by PL of L-HTL perovskite films as a function of halide choice and annealing.

In contrast, minimizing lead iodide reduces possible degradation by the photolysis of lead iodide,[29] and improving homogeneity is reported to correlate with better stability.[30]

From XRD and SEM, it appears that L-HTLs contribute to a more complete conversion to perovskite. Both examples so far used chloride-based salts. To better resolve the role of the halide in this conversion process, we measured the photoluminescence quantum yield (PLQY) of perovskite films using L-HTLs with formamidinium cations with varying halides (Figure 3g). Here, we use FA instead of MA to isolate the role of halides. The PLQY was calculated from the emitted PL from samples excited with a laser at ≈1 sun equivalent intensity (Supporting Information Methods). Additionally, these graphs show the impact on PL from annealing. Immediately after deposition, the PLQY of the sample loaded with FAI was like the control. This indicates additional FAI loading does not strongly affect the evaporation process. However, after annealing the additional material appears to react, as the PLQY became superior to the control. Control samples often lose a portion of their PL intensity from annealing. Bromide and chloride loading behaved differently, where the PLQY was higher than the control immediately after deposition. Bromide- and chloride-based precursors appear to actively incorporate into the film during the deposition process, as the PLQY was higher than the control before annealing. Additionally, we see that the PLQY increased after annealing. This suggests that these precursors are only partially converted to perovskite during deposition, and the rest is incorporated during annealing. We expected that chlorine aids perovskite film growth yielding higher PLQY,[31] and indeed we see films loaded with FACl showed a higher PLQY than those loaded with FAI (Figure 3g). For this batch, all films had a similar reduction in bandgap from annealing (Figure 3h).

We fabricated solar cells using HTLs loaded with MACl and FBACl. The molecule FBACl was chosen as a typical representative of the bulky cations used for the formation of low-D perovskites. We expected both materials to improve our PLQY, resulting in a higher open circuit voltage (V_{OC}) for solar cells. In Figure S3, Supporting Information, we show films loaded with 2 concentrations of 4 and 16 mM for both materials. The concentration of MeO-2PACz was 4 mM. The higher concentration of 16 mM was used to see if adding a significant molar excess interferes with the function of the HTL. Both precursors (MACl and FBACl) can increase the V_{OC} when added at 4 mM concentrations. Using higher concentrations of MACl caused the V_{OC} to abruptly drop. This drop in V_{OC} did not happen for the FBACl. We conclude that a monolayer of MeO-2PACz can self-assemble and bind to the ITO surface, even as a minority solute. However, too high a concentration of MACl may take the film outside the range of optimal performance, as seen here using 16 mM MACl.

Both MACl and FBACl treatments improved the short circuit current (J_{SC}). The bandgap of the 4 mM FBACl and 4 mM MACl samples were both 1.65 eV, which were both higher than that of the control ≈1.64 eV. This indicates that the J_{SC} improvement was not a result of bandgap change. This was especially surprising for the FBACl as we primarily anticipated an improved V_{OC}. Films using MACl and FBACl both appear visibly darker suggesting an improvement in the absorption coefficient. To clearly illustrate how an L-HTL can impact absorption we show the external quantum efficiency (EQE) of a batch where the control appeared to be deficient in FAI. In this batch, the films grown with an L-HTL had significantly improved J_{SC} from increased absorption (Figure S4, Supporting Information).

Additionally, adding either MACl or FBACl improved the apparent shunt resistance. If we disregard cells with obvious shunts and measure the shunt resistance from the slope of *J–V* curves at short-circuit we see that the average shunt resistance is more than twice as high as that of the control (1.7, 1.4, and 0.6 Ω cm^2 for the MACl, FBACl, and control). This improved shunt resistance is one factor leading to the improved fill factor (FF) for L-HTLs. The exact origin of the poor shunt resistance from the control perovskite is not certain but may originate from the interface between the perovskite and HTL. One caveat about the use of FBACl is that it increases the hysteresis.

We tried adding both materials concurrently to see if improvements were constructive. We kept the concentration of MACl at 4 mM but limited the concentration of FBACl to 0.6 mM to reduce hysteresis. The results appear largely constructive and are shown in **Figure 4** and **Table 1**. The loaded perovskite solar cells have substantially increased J_{SC}. The loaded samples had a higher average and maximum V_{OC} than the control. However, the V_{OC} was not higher for all cells, which may partially originate from the control (1.64 eV) having a larger bandgap than the L-HTL ≈1.63 eV. The reduced bandgap could also explain some of the increase in J_{SC} for the L-HTL film. The L-HTL cells showed improvement in the shunt resistance compared to the control (1.2 versus 0.7 Ω cm^2). This improved shunt resistance contributed to an overall improvement in the FF. The net result is a substantial improvement in PCE, with peak performers going from ≈17% to over 19% for L-HTL films.

We measured the PL of the films used to prepare devices in Figure 4 at different stages of fabrication, immediately after evaporation, after annealing, and a complete solar cell with C_{60} and Bathocuproine (BCP). Additionally, we estimated the quasi-fermi level splitting at these stages of fabrication and compared values to the V_{OC} measured from complete solar cells (Figure S5, Supporting Information).

C_{60} can quench the PL of perovskite films and limit V_{OC}. The molecule ethylenediammonium diiodide ($EDAI_2$) is reported as an evaporated surface treatment between perovskite and C_{60} that improves the V_{OC}.[32] We treated one substrate with $EDAI_2$ and compared it to another film prepared in the same evaporation. Both substrates used an L-HTL with 4 mM MACl and 0.6 mM FBACl. Improvements in V_{OC} are reportedly from n doping the perovskite, preventing the quenching of hole carriers of the perovskite by C_{60}.[32] In this batch, we saw some improvement in V_{OC} and PCE from the $EDAI_2$ treatment. However, in this example, there was a slight loss in FF. The champion cell of this batch showed a PCE of ≈19.1% under maximum power point (MPP) tracking for 5 min. A second evaporation using an $EDAI_2$ treatment is shown in Figure S6, Supporting Information. These samples showed a more pronounced impact on the V_{OC} and no loss in FF from $EDAI_2$ (Table S2, Supporting Information). Additionally, $EDAI_2$ can increase the PLQY of films independent of interaction with C_{60} (Figure S7, Supporting Information) and likely provides a multifunctional improvement for V_{OC}.

To probe charge transfer between the perovskite and the ITO, we measured the time-resolved surface photovoltage (TRSPV) of perovskite thin films (Figure S8a, Supporting Information). There is a published model of the TRSPV response for perovskite on carbazole-based SAMs.[33] This model identifies 5 significant features, which are defined by surface trap density at the HTL and relevant rate constants. First, (i) there is an initial positive signal corresponding to electron trapping at the surface. (ii) This is followed by a rapid rise of a negative signal associated with hole extraction into the ITO/HTL layer. (iii) The decay of this initial negative pulse i defined by the rate of electron–hole recombination. (iv) A secondary shoulder can arise from detrapping electrons bound at the perovskite-HTL interface. (v) The final signal decay is defined by the recombination of these detrapped electrons, and potentially holes that re-enter the perovskite from the ITO/HTL layer. This publication also notes that MeO-2PACz has a noticeable signal from electron detrapping (iii).

We measured TRSPV on 3 samples, a control film with only perovskite on MeO-2PACz, a film using an L-HTL with 4 mM MACl, and an L-HTL using 1 mM FBACl. The hole extraction (ii) appears comparable for the control and MACl samples. However, the signal from FBACl is smaller suggesting a reduced rate of hole extraction. This reduced rate of hole extraction could explain the hysteresis seen in some FBACl samples. The rate of recombination (iii) is slower for the MACL and FBACl samples, with a slope that is approximately half that of the control. The most significant difference from the control sample appears in the second peak associated with electron detrapping (iv), where the MACl and FBACl samples appeared to de-trap an order of magnitude sooner (≈10 versus ≈100 µs) and with a larger signal than the control. Reduced recombination and a faster onset of detrapping may indicate fewer or shallower traps. These improvements could correlate with the improved FF seen in devices using MACl and FBACl.

To complement the TRSPV data, we measured time-resolved photoluminescence (TRPL) for the same 3 films (Figure S8b, Supporting Information). For short time scales (≈10^{-9} s), the FBACl sample produces higher PL, possibly from a reduced rate of hole extraction. At longer time scales (≈10^{-8} to ≈10^{-7} s), we see higher PL from MACl and FBACl. The MACl sample appeared to have a similar rate of hole extraction as the control, so reduced non-radiative recombination is a likely source of the PL increase. At ≈10^{-6} s, we see a change in the slope of PL decay, which could be the onset of electron detrapping, which causes a more rapid decay in PL. We do not see such a change for the control, which may not see de-trapping until much later.

Combining all treatments (6 mM MACl, 0.6 mM FBACl, and 0.3 nm of $EDAI_2$), we reached an efficiency of 20.3% compared to the 18.0% of the best cell of the control evaporated in the same batch (**Figure 5**). This cell using an L-HTL had a higher J_{SC} than the control (23.8 versus 21.9 mA cm^{-2}), which was

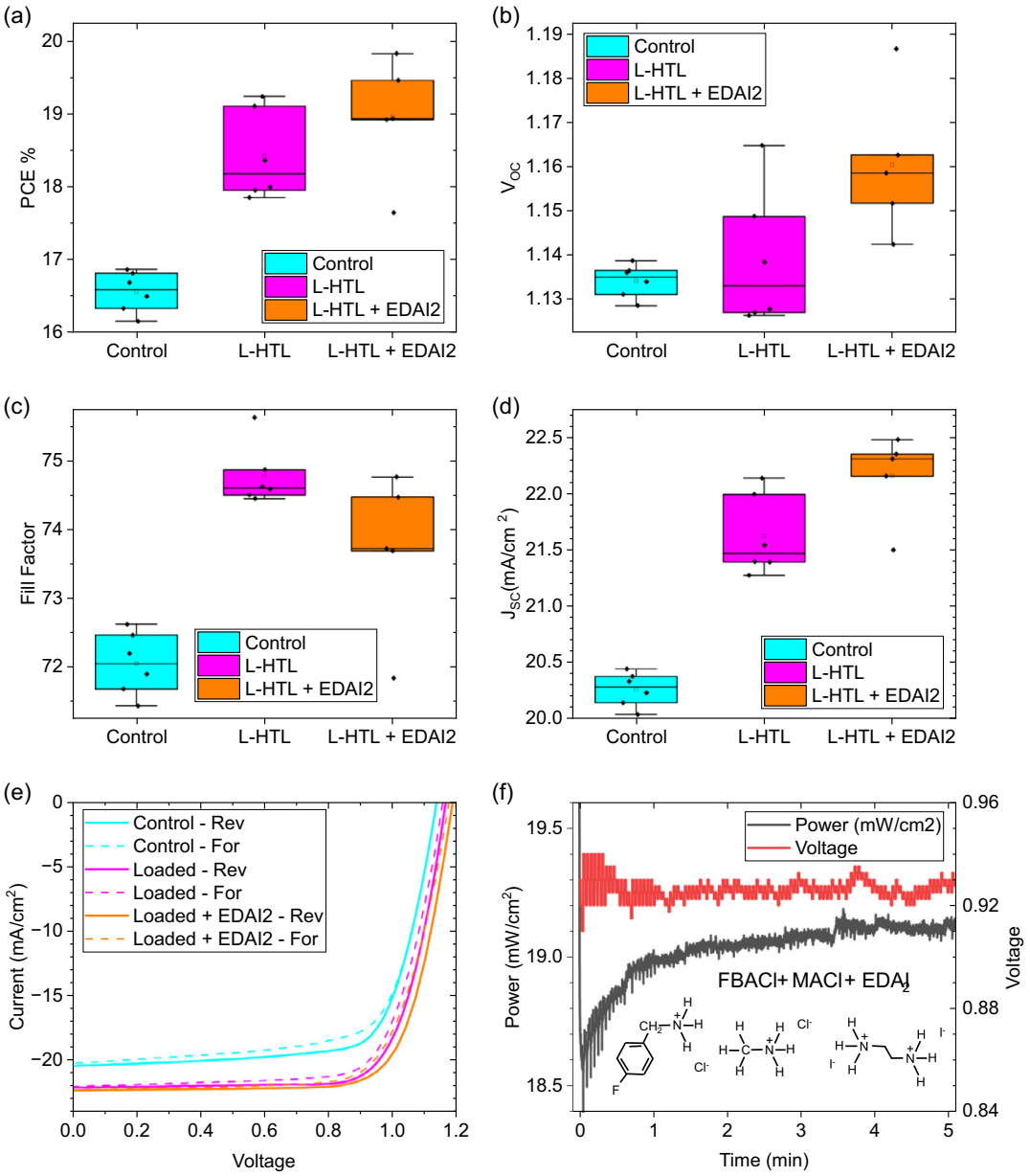

Figure 4. Loading multiple precursors (MACl and FBACl) concurrently in HTLs can provide constructive improvements in solar cell performance. a–d) Box plots of PCE, V_{OC}, FF, and J_{SC} from the reverse scans of different loaded substrates, all prepared during the same evaporation. e) JV scan from the best cells of each substrate. f) MPP tracking for the champion cell of this evaporation using 4 mM MACl, 0.6 mM FBACl, and $EDAI_2$.

Table 1. Solar cell performance for cells, as shown in Figure 4, displaying the average of forward and reverse scans and standard deviations for the substrate. The highest values for each substrate are shown in parentheses.

	J_{SC} [mA cm^{-2}]	V_{OC}	FF	PCE [%]	R_{Shunt} [Ω cm^{-2}]
Control	20.2 ± 0.2 (20.4)	1.13 ± 0.004 (1.14)	70.6 ± 1.6 (72.6)	16.1 ± 0.5 (16.8)	0.75 ± 0.30 (1.11)
L-HTL	21.5 ± 0.4 (22.1)	1.14 ± 0.14 (1.16)	73.0 ± 2.1 (75.6)	17.9 ± 0.9 (19.2)	1.20 ± 0.79 (2.91)
L-HTL + $EDAI_2$	22.1 ± 0.4 (22.5)	1.16 ± 0.14 (1.18)	72.6 ± 1.5 (74.8)	18.6 ± 0.8 (19.8)	2.38 ± 0.86 (3.71)

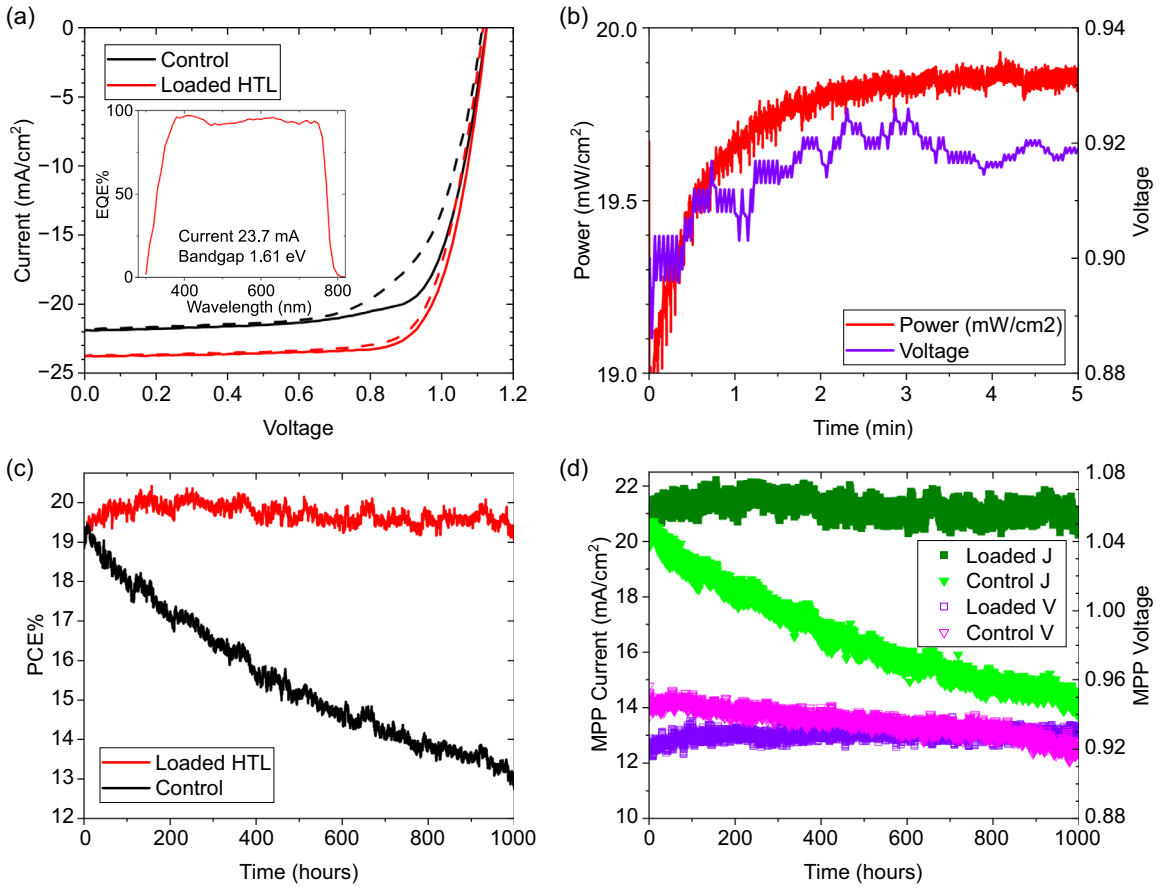

Figure 5. Perovskite solar cells using an L-HTL (MACl, FBACl) and an $EDAI_2$ surface treatment show improved efficiency and stability. a) The champion cell using the L-HTL had a max PCE of 20.3% as measured by JV scan, compared to the 18.0% for the control. The integrated current density from EQE (23.7 mA cm^{-2}) approximately matched the current density from the JV scan. b) MPP tracking after initial JV scans shows ≈19.9% PCE operating at ≈0.92 volts. c,d) Long-term MPP tracking, where the most stable cell from each substrate is shown. The peak efficiency for the L-HTL and control cells were ≈20.3% and ≈19.4%. The T_{90} lifetime for control was ≈170 h, while the sample using an L-HTL did not decay below its initial value within the first 1000 h. d) Voltage and current values for both samples during the 1000 h of MPP tracking.

corroborated by EQE (Figure 5a), which gave an integrated J_{SC} of 23.7 mA cm^{-2}. The cell with an L-HTL had a comparable V_{OC} (1.13) to the control despite having a lower bandgap as measured by PL (Control 1.65 eV, and L-HTL ≈1.62 eV). We measured these cells after initial JV scans by MPP tracking for 5 min, which gave a PCE of ≈19.9% operated at ≈0.92 volts. Gains from using an L-HTL and $EDAI_2$ consistently outperform the control samples within the same batch. Both L-HTL and control samples from this batch were taken to a secondary setup for long-term MPP tracking. In Figure 5b,c, we show the most stable cell from each substrate. The cell using an L-HTL was more stable than the control. We will quantify this stability with the time to reach 90% of peak efficiency (T_{90}). The control rose in efficiency from 18% to a peak of ≈19.4% at ≈10 h. The PCEs shown in long-term MPP are only approximate, as the MPP solar simulator was not an A-grade spectral match. This control cell decayed to 90% of its peak efficiency at ≈170 h. We do not directly see the T_{90} point on our cell using an L-HTL in the first 1000 h, as efficiencies were still higher than its initial value. A rough estimate of the T_{90} (≈3500 h) is provided in the supporting information. Comparing JV scans before and after 1000 h of MPP, the control cell lost both J_{SC} and FF but maintained its V_{OC}. The L-HTL sample increased in V_{OC}, but slightly decreased in FF. A table summarizing the changes in the samples from Figure 5 is shown in Table S3, Supporting Information. Additionally, there is a table of normalized efficiency for all cells used for MPP tracking. We show relative performance by comparing our results to those from the perovskite database (Figure S9, Supporting Information).[34] A champion solar cell using a substrate with an antireflection coating, but otherwise similar conditions, reached a PCE of 21% as measured by JV and MPP (Figure S10, Supporting Information).

Such a large difference in stability is surprising for samples concurrently evaporated with similar starting efficiencies. However, these samples appear to have important differences which influence decay. Likely factors include the significant excess of lead iodide in the control sample, which can reduce stability via the decomposition of lead iodide to lead metal.[17,29] The control sample also had an increased proportion of the hexagonal phase (6 H) perovskite, which is also linked to rapid decomposition.[22] The L-HTL sample had a small fraction of FBA cation which we believe should passivate surface defects

and slow decay.[15] In aggregate, the stability improvement for the L-HTL sample was pronounced, despite the relatively small fractional change in total material (<1%).

3. Conclusion

We showed that by using L-HTLs, we incorporated materials into coevaporated lead halide perovskites that may otherwise be only accessible to solution-processed films. We demonstrated the inclusion of MACl, and the inclusion of small fractions of the low-D cation FBA. Using L-HTLs, perovskite films had a more complete conversion of lead halide to perovskite and higher PLQY. We demonstrated improved V_{OC} for solar cells using the additional evaporated surface treatment of $EDAI_2$. The films using L-HTLs and $EDAI_2$ consistently improved the efficiency of solar cells compared to the best control samples evaporated concurrently. L-HTLs improved most relevant metrics, including J_{SC}, FF, and V_{OC}. Solar cells using L-HTLs and $EDAI_2$ demonstrated stability where cells did not decay below their initial PCE after 1000 h of MPP-tracking under AM1.5-equivalent illumination. A champion cell using an L-HTL and an antireflection coating reached 21% PCE. Thus, this method is a tool that can lead to greater flexibility and improved performance in future evaporated perovskite materials.

Supporting Information

Supporting Information is available from the Wiley Online Library or from the author.

Acknowledgements

This work was funded by the following grants: 03EE1086C (PrEsto), 03EE1123 A-E (SHAPE), and Zeitenwende funded by HGF. Additionally, the authors would like to thank Yanyan Duan for her help with antireflection-coated ITO substrates.

Conflict of Interest

The authors declare no conflict of interest.

Author Contributions

Matthew R. Leyden: Conceptualization (lead); Formal analysis (lead); Investigation (lead); Methodology (lead); Writing—original draft (lead); Writing—review and editing (lead). **Viktor Škorjanc**: Investigation (supporting); Methodology (supporting). **Aleksandra Miaskiewicz**: Investigation (supporting); Methodology (supporting). **Stefanie Severin**: Investigation (supporting); Methodology (supporting). **Suresh Maniyarasu**: Investigation (supporting); Methodology (supporting). **Thomas Gries**: Investigation (supporting); Methodology (supporting). **Johannes Beckedahl**: Investigation (supporting); Methodology (supporting). **Florian Scheler**: Methodology (supporting). Philippe Holzhey: Formal analysis (supporting). **Jona Kurpiers**: Investigation (supporting); Methodology (supporting). **Lars Korte**: Project administration (supporting); Writing—review and editing (supporting). **Marcel Roß**: Investigation (supporting); Methodology (supporting); Project administration (supporting); Writing—review and editing (supporting). **Steve Albrecht**: Funding acquisition (lead); Project administration (lead); Writing—review and editing (lead). **Maxim Simmonds**: Investigation (supporting).

Data Availability Statement

The data that support the findings of this study are available from the corresponding author upon reasonable request.

Keywords

coevaporation, perovskites, solar cells

Received: August 5, 2024
Revised: September 12, 2024
Published online: October 2, 2024

[1] S. Akel, A. Kulkarni, U. Rau, T. Kirchartz, *PRX Energy* **2023**, *2*, 013004.
[2] NREL, *Best Research-Cell Efficiency Chart*, https://www.nrel.gov/pv/cell-efficiency.html.
[3] S. Liu, J. Li, W. Xiao, R. Chen, Z. Sun, Y. Zhang, X. Lei, S. Hu, M. Kober-Czerny, J. Wang, F. Ren, Q. Zhou, H. Raza, Y. Gao, Y. Ji, S. Li, H. Li, L. Qiu, W. Huang, Y. Zhao, B. Xu, Z. Liu, H. J. Snaith, N.-G. Park, W. Chen, *Nature* **2024**, 1.
[4] L. Gil-Escrig, C. Dreessen, F. Palazon, Z. Hawash, E. Moons, S. Albrecht, M. Sessolo, H. J. Bolink, *ACS Energy Lett.* **2021**, *6*, 827.
[5] S. Mariotti, E. Köhnen, F. Scheler, K. Sveinbjörnsson, L. Zimmermann, M. Piot, F. Yang, B. Li, J. Warby, A. Musiienko, D. Menzel, F. Lang, S. Keßler, I. Levine, D. Mantione, A. Al-Ashouri, M. S. Härtel, K. Xu, A. Cruz, J. Kurpiers, P. Wagner, H. Köbler, J. Li, A. Magomedov, D. Mecerreyes, E. Unger, A. Abate, M. Stolterfoht, B. Stannowski, R. Schlatmann, L. Korte, S. Albrecht, *Science* **2023**, *381*, 63.
[6] M. Roß, S. Severin, M. B. Stutz, P. Wagner, H. Köbler, M. Favin-Lévêque, A. Al-Ashouri, P. Korb, P. Tockhorn, A. Abate, B. Stannowski, B. Rech, S. Albrecht, *Adv. Energy Mater.* **2021**, *11*, 2101460.
[7] https://www.epa.gov/sites/default/files/2016-09/documents/n-n-dimethylformamide.pdf.
[8] https://www.epa.gov/sites/default/files/2016-09/documents/chlorobenzene.pdf.
[9] D. P. Mcmeekin, P. Holzhey, S. O. Fürer, S. P. Harvey, L. T. Schelhas, J. M. Ball, S. Mahesh, S. Seo, N. Hawkins, J. Lu, M. B. Johnston, J. J. Berry, U. Bach, H. J. Snaith, *Nat. Mater.* **2023**, *22*, 73.
[10] X. Zhao, W. Gao, H. Dong, Y. Zhou, H. Huang, Z. Wu, C. Ran, *Nano Energy* **2024**, *128*, 109933.
[11] T. Abzieher, D. T. Moore, M. Roß, S. Albrecht, J. Silvia, H. Tan, Q. Jeangros, C. Ballif, M. T. Hoerantner, B.-S. Kim, H. J. Bolink, P. Pistor, J. C. Goldschmidt, Y.-H. Chiang, S. D. Stranks, J. Borchert, M. D. Mcgehee, M. Morales-Masis, J. B. Patel, A. Bruno, U. W. Paetzold, *Energy Environ. Sci.* **2024**, *17*, 1645.
[12] J. Zhou, L. Tan, Y. Liu, H. Li, X. Liu, M. Li, S. Wang, Y. Zhang, C. Jiang, R. Hua, W. Tress, S. Meloni, C. Yi, *Joule* **2024**, *8*, 1961.
[13] M. Kroll, S. D. Öz, Z. Zhang, R. Ji, T. Schramm, T. Antrack, Y. Vaynzof, S. Olthof, K. Leo, *Sustain. Energy Fuels* **2022**, *6*, 3230.
[14] M. Roß, M. B. Stutz, S. Albrecht, *Sol. RRL* **2022**, *6*, 2200500.
[15] Y. Liu, S. Yuan, H. Zheng, M. Wu, S. Zhang, J. Lan, W. Li, J. Fan, *Adv. Energy Mater.* **2023**, *13*, 2300188.
[16] A. Al-Ashouri, A. Magomedov, M. Roß, M. Jošt, M. Talaikis, G. Chistiakova, T. Bertram, J. A. Márquez, E. Köhnen, E. Kasparavičius, S. Levcenco, L. Gil-Escrig, C. J. Hages, R. Schlatmann, B. Rech, T. Malinauskas, T. Unold, C. A. Kaufmann, L. Korte, G. Niaura, V. Getautis, S. Albrecht, *Energy Environ. Sci.* **2019**, *12*, 3356.
[17] Y. Gao, F. Ren, D. Sun, S. Li, G. Zheng, J. Wang, H. Raza, R. Chen, H. Wang, S. Liu, P. Yu, X. Meng, J. He, J. Zhou, X. Hu, Z. Zhang, L. Qiu, W. Chen, Z. Liu, *Energy Environ. Sci.* **2023**, *16*, 2295.

[18] T. Feeney, J. Petry, A. Torche, D. Hauschild, B. Hacene, C. Wansorra, A. Diercks, M. Ernst, L. Weinhardt, C. Heske, G. Gryn'ova, U. W. Paetzold, P. Fassl, *Matter* **2024**, *7*, 2066.
[19] https://www.sigmaaldrich.com/DE/en/sds/mm/8.06020?userType=anonymous.
[20] L. Mao, W. Ke, L. Pedesseau, Y. Wu, C. Katan, J. Even, M. R. Wasielewski, C. C. Stoumpos, M. G. Kanatzidis, *J. Am. Chem. Soc.* **2018**, *140*, 3775.
[21] P. Gratia, I. Zimmermann, P. Schouwink, J.-H. Yum, J.-N. Audinot, K. Sivula, T. Wirtz, M. K. Nazeeruddin, *ACS Energy Lett.* **2017**, *2*, 2686.
[22] S. Macpherson, T. A. S. Doherty, A. J. Winchester, S. Kosar, D. N. Johnstone, Y.-H. Chiang, K. Galkowski, M. Anaya, K. Frohna, A. N. Iqbal, S. Nagane, B. Roose, Z. Andaji-Garmaroudi, K. W. P. Orr, J. E. Parker, P. A. Midgley, K. M. Dani, S. D. Stranks, *Nature* **2022**, *607*, 294.
[23] X. Shen, B. M. Gallant, P. Holzhey, J. A. Smith, K. A. Elmestekawy, Z. Yuan, P. V. G. M. Rathnayake, S. Bernardi, A. Dasgupta, E. Kasparavicius, T. Malinauskas, P. Caprioglio, O. Shargaieva, Y. Lin, M. M. Mccarthy, E. Unger, V. Getautis, A. Widmer-Cooper, L. M. Herz, H. J. Snaith, *Adv. Mater.* **2023**, *35*, 2211742.
[24] E. L. Unger, L. Kegelmann, K. Suchan, D. Sörell, L. Korte, S. Albrecht, *J. Mater. Chem. A* **2017**, *5*, 11401.
[25] M. R. Leyden, T. Matsushima, C. Qin, S. Ruan, H. Ye, C. Adachi, *Phys. Chem. Chem. Phys.* **2018**, *20*, 15030.
[26] D. R. Wargulski, K. Xu, H. Hempel, M. A. Flatken, S. Albrecht, D. Abou-Ras, *ACS Appl. Mater. Interfaces* **2023**, *15*, 41516.
[27] M. R. Leyden, L. K. Ono, S. R. Raga, Y. Kato, S. Wang, Y. Qi, *J. Mater. Chem. A* **2014**, *2*, 18742.
[28] Y.-H. Chiang, M. Anaya, S. D. Stranks, *ACS Energy Lett.* **2020**, *5*, 2498.
[29] G. Tumen-Ulzii, C. Qin, D. Klotz, M. R. Leyden, P. Wang, M. Auffray, T. Fujihara, T. Matsushima, J. Lee, S. Lee, Y. Yang, C. Adachi, *Adv. Mater.* **2020**, *32*, 1905035.
[30] Y. Bai, Z. Huang, X. Zhang, J. Lu, X. Niu, Z. He, C. Zhu, M. Xiao, Q. Song, X. Wei, C. Wang, Z. Cui, J. Dou, Y. Chen, F. Pei, H. Zai, W. Wang, T. Song, P. An, J. Zhang, J. Dong, Y. Li, J. Shi, H. Jin, P. Chen, Y. Sun, Y. Li, H. Chen, Z. Wei, H. Zhou, Q. Chen, *Science* **2022**, *378*, 747.
[31] K. B. Lohmann, S. G. Motti, R. D. J. Oliver, A. J. Ramadan, H. C. Sansom, Q. Yuan, K. A. Elmestekawy, J. B. Patel, J. M. Ball, L. M. Herz, H. J. Snaith, M. B. Johnston, *ACS Energy Lett.* **2022**, *7*, 1903.
[32] S. Hu, J. Pascual, W. Liu, T. Funasaki, M. A. Truong, S. Hira, R. Hashimoto, T. Morishita, K. Nakano, K. Tajima, R. Murdey, T. Nakamura, A. Wakamiya, *ACS Appl. Mater. Interfaces* **2022**, *14*, 56290.
[33] I. Levine, A. Al-Ashouri, A. Musiienko, H. Hempel, A. Magomedov, A. Drevilkauskaite, V. Getautis, D. Menzel, K. Hinrichs, T. Unold, S. Albrecht, T. Dittrich, *Joule* **2021**, *5*, 2915.
[34] T. J. Jacobsson, A. Hultqvist, A. García-Fernández, A. Anand, A. Al-Ashouri, A. Hagfeldt, A. Crovetto, A. Abate, A. G. Ricciardulli, A. Vijayan, A. Kulkarni, A. Y. Anderson, B. P. Darwich, B. Yang, B. L. Coles, C. A. R. Perini, C. Rehermann, D. Ramirez, D. Fairen-Jimenez, D. Di Girolamo, D. Jia, E. Avila, E. J. Juarez-Perez, F. Baumann, F. Mathies, G. S. A. González, G. Boschloo, G. Nasti, G. Paramasivam, G. Martínez-Denegri, H. Näsström, H. Michaels, H. Köbler, H. Wu, I. Benesperi, M. I. Dar, I. Bayrak Pehlivan, I. E. Gould, J. N. Vagott, J. Dagar, J. Kettle, J. Yang, J. Li, J. A. Smith, J. Pascual, J. J. Jerónimo-Rendón, J. F. Montoya, J.-P. Correa-Baena, J. Qiu, J. Wang, K. Sveinbjörnsson, K. Hirselandt, K. Dey, K. Frohna, L. Mathies, L. A. Castriotta, M. H. Aldamasy, M. Vasquez-Montoya, M. A. Ruiz-Preciado, M. A. Flatken, M. V. Khenkin, M. Grischek, M. Kedia, M. Saliba, M. Anaya, M. Veldhoen, N. Arora, O. Shargaieva, O. Maus, O. S. Game, O. Yudilevich, P. Fassl, Q. Zhou, R. Betancur, R. Munir, R. Patidar, S. D. Stranks, S. Alam, S. Kar, T. Unold, T. Abzieher, T. Edvinsson, T. W. David, U. W. Paetzold, W. Zia, W. Fu, W. Zuo, V. R. F. Schröder, W. Tress, X. Zhang, Y.-H. Chiang, Z. Iqbal, Z. Xie, E. Unger, *Nat. Energy* **2022**, *7*, 107.